Silo flow and clogging in the presence of an obstacle

Anna Belle Harada, Emma Thackray, and Kerstin N. Nordstrom*
Department of Physics, Mount Holyoke College, South Hadley, Massachusetts 01075, USA

(Received 4 November 2021; accepted 3 May 2022; published 26 May 2022)

In this work we present experimental results of the flow and clogging of monodisperse spheres in a silo geometry, with an obstacle placed near the exit aperture. In previous work, it has been shown that the placement of an obstacle in a two-dimensional silo can suppress clogging. We extend prior work to investigate the effects of obstacle size, and find that larger obstacles are better at suppressing clogs; however, most obstacles will suppress clogging. We investigate the local velocity, granular temperature, and local packing for several specific cases, and find that the mechanisms of clog suppression may be different depending on the exact size of the obstacle, with one case not suppressing clogs at all. We find bulk granular temperatures are increased with the presence of an obstacle, but local temperatures near the exit may not be. We also find the average packing is not substantially affected by an obstacle, but the local packing can be quite different. Specifically, large obstacles introduce spatial disorder that percolates, resulting in a more fluid system overall. We also observe spatiotemporal inhomogeneity in the flows.

DOI: 10.1103/PhysRevFluids.7.054301

I. INTRODUCTION

The flow of granular material through a silo or hopper has been studied for many years. In addition to its great practical importance in many industrial processing situations, it is also displays a number of intriguing flow characteristics. While empirical rules for flow have been around for some time [1], a satisfying fundamental predictive model for flow and clogging has remained elusive. Recently, interest in these systems has resurfaced for a number of reasons. For starters, advances in computing and high-speed imaging have made it possible to study the microscopics of flows [2–4], and even techniques such as MRI and CT scanning have been employed [5,6]. Further, many are interested in the connection of clogging to the jamming transition [7,8] and the connection of clogging to other kinds of bottleneck flows, such as pedestrian egress and traffic bottlenecks [9–11].

The general phenomenology of gravity-driven silo flow is simple. There appears to be a transitional exit aperture size, about five grain diameters. The precise value varies from system to system, but the phenomenon is general. When the exit aperture is larger than this transitional size, particles will flow continuously according to the Beverloo law, with a rate that is independent of filling height, provided the fill height is adequate and the silo width is large enough compared to the aperture and grain diameters [12]. This precise flow rate will vary slightly from system to system, but the functional form holds over a wide array of systems. When the aperture is smaller than this transitional size, particles will form a clog with some likelihood [13,14]. In the infinitely tall silo limit (or if experimentally one can resupply particles at the top), this means any silo with a small aperture will clog eventually. There is no way to predict when this clog will occur, but larger aperture sizes will have larger average discharge events before a clog [15]. There is controversy in

*Corresponding author: knordstr@mtholyoke.edu

the literature about whether the transition in behavior marks a critical point, or whether the clogging transition is simply probabilistic in nature: beyond some aperture size, it becomes overwhelmingly unlikely for a clog to occur [16,17]. This paper does not aim to settle that particular debate, though the evidence increasingly points to the probabilistic nature of clogging [18].

Regardless of the true nature of the transition, systems do clog with some probability if the exit aperture is small. Intriguingly, adding an obstacle near the exit aperture has been shown to dramatically reduce the clogging probability for silo flow [19–21]. An obstacle can also enhance or suppress the flow rate, though the effect is modest (at most 10%) and there is not a systematic prediction for whether a flow will be enhanced or suppressed. Prior work has investigated this in several ways in two-dimensional (2D) systems, combining clogging measurements with microscopic measurements of particle motions. In [19], a circular obstacle of about ten particle diameters was investigated, and the distance to the exit aperture was varied. In an extension of this work [20], additional effects of the outlet size were explored. In [21], a similar obstacle size was explored, and the shapes of the obstacles were varied: circle, triangle, inverted triangle.

In this paper, we complement prior studies by looking into the additional effects of obstacle size on the clogging behavior, in tandem with varying the obstacle position. Our particles are intermediate in size between [19] and [21], and we have similar time and spatial resolution to the other studies. We perform similar measurements of velocity fields and granular temperature, and propose a more natural metric to study the packing structure of the system.

II. METHODS

We study the flow and clogging of monodisperse spheres in a quasi-2D silo in the presence of an obstacle. The silo walls are transparent to allow imaging of the particle motions.

Particles. The particles are clear acrylic spheres (Engineering Labs). They are highly monodisperse, with a size of 3.160 ± 0.002 mm, sampled by micrometer measurement. The size distribution skews to the smaller size, with no particles sampled exceeding 3.175 mm. For each experiment, we start with a filled silo, which is approximately 12 000 particles. The particles are poured into the top of the apparatus for each experimental run, and completely evacuated before pouring for new experiments.

Silo. The front and back of the silo is made with 3/8-in. static dissipative acrylic sheets (McMaster-Carr). Teflon sheeting (McMaster-Carr) was laser cut (Epilog) to make inserts to provide the appropriate sidewall and aperture geometry. For different aperture sizes, a different insert is used. An insert is sandwiched between the acrylic sheets, and holes have been tapped into the acrylic sheeting to screw the container together using set screws. The silo is then mounted onto a support frame built from t-slot aluminum, which rests on an optical table. The resulting dimensions of the silo are as follows: 200 mm wide, 475 mm tall, and 3.2 mm thick. Before a trial, testing is done with a rod of fixed diameter to ensure the gap is sufficient to allow free flow of particles, and in rare cases of any doubt, the set screws are all loosened the same small amount. This process is iterated until the gap is judged sufficient. Plugs to close the aperture while filling the silo were 3D printed (Makerbot) to specification, allowing the particles on the plug to rest flush with the other particles on the bottom. The plugs are primarily flat pieces that are inserted horizontally, and designed to be removed via a swift horizontal motion, minimizing their influence on the outflow dynamics. (If one considers the silo area to be the xy plane, the plug is inserted/removed in the z direction.) In other work, we have verified the system follows the Beverloo law [22] for flow without obstacles [1].

Obstacles. Circular obstacles are laser cut from the same Teflon sheeting used for the sidewalls. We investigate the effect of five obstacle sizes: $3D$, $5.5D$, $10D$, $17D$, and $30D$. Obstacles are fixed to the walls of the silo with double-sided tape, and are centered with respect to the aperture opening. The obstacle height H is varied, and it is measured from the exit aperture to the bottom of the obstacle, keeping with the convention in [21].

Measurements. We use a Phantom v1611 camera (Vision Research) to film flow at 1000 frames per second at a resolution of 1280×800 pixels. The system is illuminated by symmetric LED

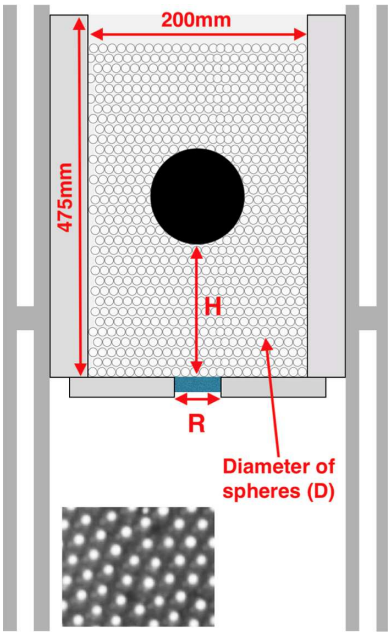

FIG. 1. A schematic of the silo used in our experiments, with relative proportions modified for clarity of presentation. A monolayer of grains is poured between two acrylic sheets. The gap between the sheets as well as the exit aperture are set by a Teflon insert sandwiched between the acrylic sheets. The apparatus is supported by aluminum framing. The aperture size is indicated by R and the obstacle height by H. Inset: An image of particles in our flow experiments. The bright spots are reflections off the particle centers used for tracking. The particles themselves are close packed.

spotlights to the sides of the camera. This results in bright reflections at the center of each particle. These reflections are used for tracking. Tracking is done via a home-built code in MATLAB, which is an adaptation of the Crocker-Grier code [23], which gives subpixel accuracy of particle positions.

III. BULK RESULTS

To measure clogging, there have been two main approaches taken in the past. One is to ask the question of "does it clog?" and take multiple trials to arrive at an expectation probability [15]. The other method is to continuously supply particles at the top as needed, and measure the avalanche size before a clog [19]. Thus the question becomes not will it clog, but "how long does it take to clog?" While the second method is more elegant, our silo is not trivial to refill without disturbing the flow, thus we must use the cruder binary metric.

In other experiments [22] we have determined our transition from free flow to clogging to be near $R = 5D$, though somewhat higher than $5D$. To study clogging statistics with obstacles, we focus on $R = 5D$. This has a clogging probability of 73% with no obstacle present. We have performed trials for various obstacle heights (H) above the aperture, defined in the same way as [21], where we measure from the bottom of the obstacle to the aperture, as depicted in Fig. 1. We study five obstacle heights in total, which are $3D$, $6D$, $8D$, $10D$, and $15D$. We see two kinds of permanent clogs form. The first kind of clog is the formation of a symmetric arch above the aperture, as shown in Fig. 2(a). (We do not see asymmetric arches for these particles, though we have in experiments with soft, frictional disks [24].) The second kind of clog we call "side-clogging"; the particles form arches between the bottom of the silo and the obstacle, and generally create arches that appear to the sides of the aperture, as shown in Fig. 2(b). It should be noted that we see alternating side clogging

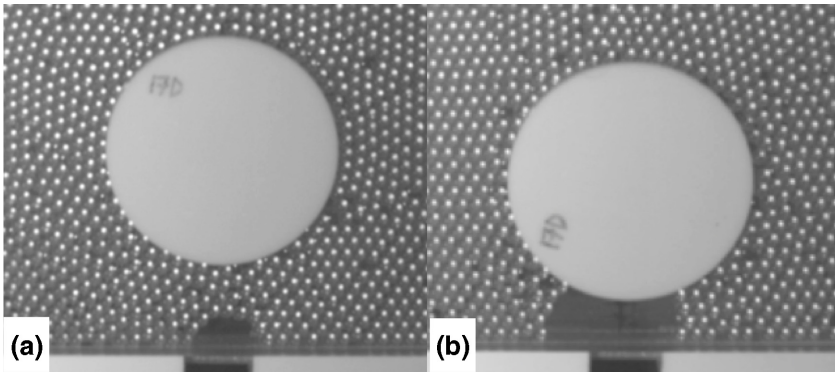

FIG. 2. Two modes of permanent clogging in the silo. (a) $17D$ obstacle, distance above $H = 8D$, shows "normal" clogging via arching over aperture. (b) $17D$ obstacle, distance above $H = 3D$, shows clogging at the sides.

during flow, meaning that one side would be clogged, while the other continues to flow. In general, these clogs were short-lived and the clogged side would unclog at some point. Often in these cases, the side that is clogged would also switch during the flow event. For our binary clogging metric, these events are not counted, but this behavior will be discussed later in this paper.

The overall results of our clogging trials are presented in Fig. 3(a), with 10 trials in general, and 20 trials for the $3D$ obstacle height. This does not represent a true "thermodynamic" limit, but gives a reliable qualitative picture of the trends. We see an overall trend that in general, larger obstacles are more effective at reducing clogging, sometimes completely reducing the probability to zero. Obstacles placed closer to the exit will also prevent clogging more readily. Both of these results could be anticipated, as bigger and closer obstacles should affect the clogging more. However, it is reassuring to see and we get a better idea for which obstacle sizes and positions are best to prevent clogging. The exception to the "closer and larger" rules occurs for obstacle size $17D$, at a distance of $3D$ above the aperture. In this case, we see a very high likelihood of clogging, where the mechanism is side-clogging.

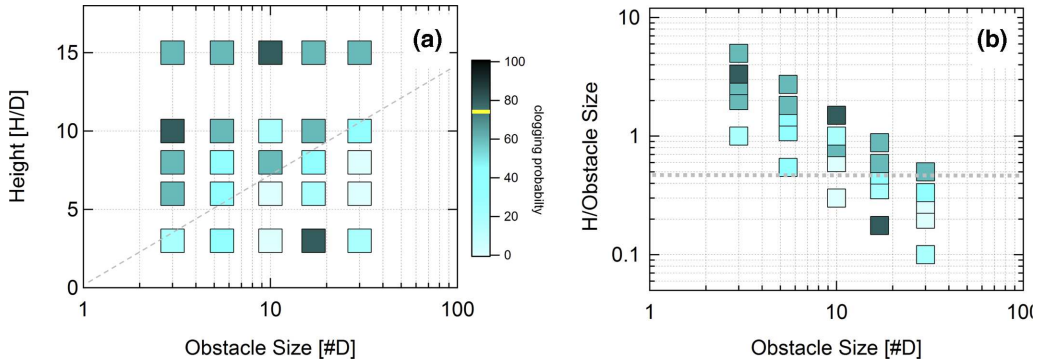

FIG. 3. (a) The clogging phase diagram for our system for aperture size $R = 5D$ and varying obstacle size and height. The clogging probability for no obstacle is 73%, indicated by the yellow line in the color bar. In general we see that clogging is reduced, and the effect is strongest for obstacles that are larger and closer to the exit aperture. The gray dashed line is a guide to the eye to divide between regimes where clogging suppression is generally better or worse. (b) The height data rescaled by obstacle size. The gray line suggests a potential rule of thumb for designing obstacle sizes.

There are are multiple relevant length scales in this scenario. However, assuming the aperture is fixed, and the particles are small compared to the obstacle, two length scales remain: the obstacle diameter and the height. Systems with the same height:diameter ratio will arguably experience self-similar boundary conditions at the obstacle. As an ansatz, we rescale the obstacle height by the obstacle diameter [Fig. 3(b)]. The dashed gray line goes through the points where no clogging occurs in the presence of an obstacle. We hypothesize this might be a good rule of thumb for producing an obstacle that is effective in reducing clogging: the obstacle height should be about $1/2$ of the obstacle radius. This is a future investigation. This also points to the limit of validity for using an obstacle: For the next smallest obstacle ($5.5D$), using this rule would put the obstacle less than two particle diameters from the aperture, which would likely create its own bottlenecks. On the other hand, there does not seem to be an inherent limit the other way, aside from insuring the obstacle is sufficiently smaller than the silo width.

In general, we arrive at a similar conclusion to prior studies [19,20]. An obstacle of approximately ten particle diameters placed closed to the aperture is extremely effective at reducing clogging; in fact, we did not see any permanent clogging in this scenario. We also note that this is in (slight) disagreement with the results of [21], as they found some clogging at small heights, though slightly higher obstacles did suppress clogging effectively. It is not known if this is simply a case of not taking enough trials (they took only three per condition) or if it has something to do with system particulars, such as particle size (their particles are approximately twice the size as ours) or composition.

We also see that an obstacle placed too close to the aperture can create other clogging opportunities at the sides. It is trivial to see why obstacles too close to the aperture might form clogs—they can effectively create a new bottleneck. Perplexingly though, a very large obstacle placed quite close to the aperture will create quite a long bottleneck region, which naively one would think should clog. However, this system (obstacle size $30D$, height $3D$) rarely clogs. Further, what is still unclear is how obstacles suppress clogging in the first place. Is their primary effect one of geometry, in that they stymie arch formation? Or is it one of dynamics, in that they alter particle trajectories? Is it a complement of both? Are there other factors worth considering? We investigate these questions by probing the microscopic particle behavior in the next section.

IV. MICROSCOPIC BEHAVIOR

For this investigation, we focus on four relevant cases of interest. We specifically choose experiments in which clogging does not happen: (1) without any obstacle, (2) with the $10D$ obstacle closest to the aperture, (3) with the $17D$ obstacle closest to the aperture, and (4) with the $30D$ obstacle closest to the aperture. We hypothesize that the mechanisms of clog suppression might be different for cases (2) and (4), as the intermediate obstacle size (case 3 at $17D$) creates a bottleneck which makes clogging extremely likely for this same height.

We measure velocity fields and the average speed vs time for the first 2.5 s of each flow, using the particle tracking data. The actual flows last 30 s; but the dynamics do not appreciably change after the startup period. We restrict our field of interest to the bottom portion of the silo, as the top portion of the silo does not undergo any particularly interesting dynamics, and certainly does not affect the exit dynamics.

We also characterize the horizontal granular temperature as a function of time, defined as $T_{gx} = \langle \delta v_x^2 \rangle = \langle (v_x - \langle v_x \rangle)^2 \rangle$ [21]. We consider this quantity for the bottom of the silo as well as for a specific region near the exit, which has a width of $10D$ (centered at the aperture) and a height of $4D$. This region corresponds to particles that are either exiting or would form clogs. This region is illustrated in Figs. 4(a) and 6(a) in green.

The last metric that we look into is related to the packing fraction of the system. However, as this is inherently an inhomogeneous and finite-sized system, the packing fraction itself is not a reliable measurement. Moreover, it would be enlightening to get a map of the spatial structure of the packing, which one does not get by calculating a simple packing fraction. To solve both problems, we take

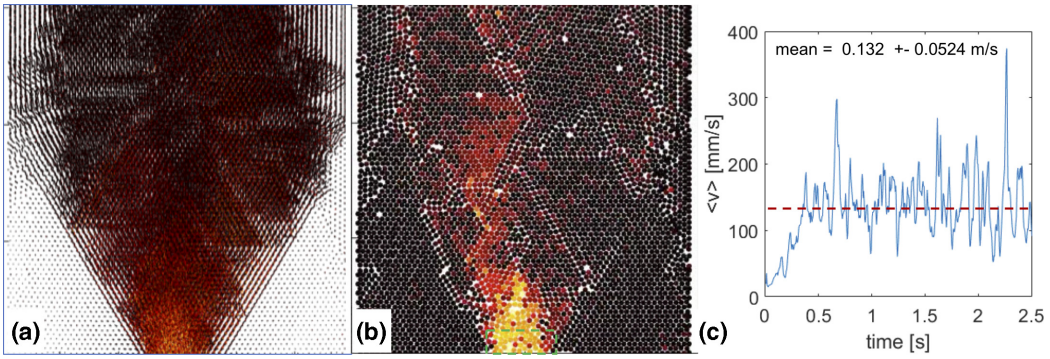

FIG. 4. (a) Tracks for 2.5 s of flow in the no obstacle experiment, overlain to show the particle movement and active/inactive regions. (b) Instantaneous speed at $t = 1$ s, with the same color scale. The dashed green box indicates the "exit" region. (c) Average particle speed vs time for the no obstacle experiment.

advantage of the monodispersity of this system and look at the local packing structure for each particle. For each particle, we search within $1.1D$ and count its neighbors in this region. If a particle has six close neighbors, it is most likely in a hexagonal packing configuration, which is the closest packed it can be. For any other neighbor count the particle is likely in a configuration with free space; clearly fewer neighbors corresponds to more free space. The strength of this measurement is ironically in its weakness, while there is ample literature regarding contact coordination number and packing fraction; see, for instance [25], we can make no claim about particle contacts: this is experimental data based on images alone. However, this metric only requires position data, it does not even require frame-to-frame tracking, just positions (an advantage, practically speaking) and based on our results, proves useful for understanding the local packing structure. We measure this for all particles in all frames, and report representative spatial images as well as averages for both the bottom of the silo and the region near the exit aperture.

Case 1: No obstacle. The velocity field is shown in Fig. 4. In Fig. 4(a), tracks are overlain to show the particle motion. We see in general most motion occurs near the aperture, but the overall flow

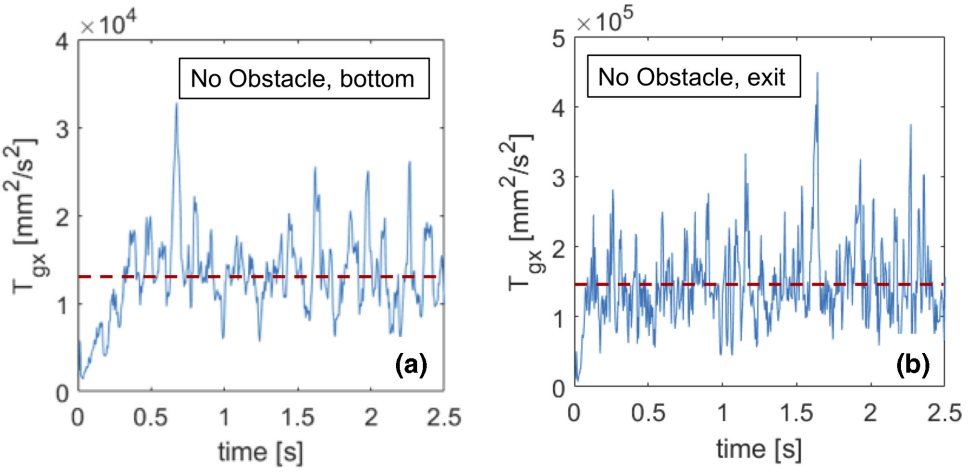

FIG. 5. (a) The horizontal granular temperature at the bottom of the silo. The mean value is $(1.31 \pm 0.481) \times 10^4$ mm^2/s^2. (b) The horizontal granular temperature at the exit of the silo. The mean value is $(1.46 \pm 0.606) \times 10^5$ mm^2/s^2.

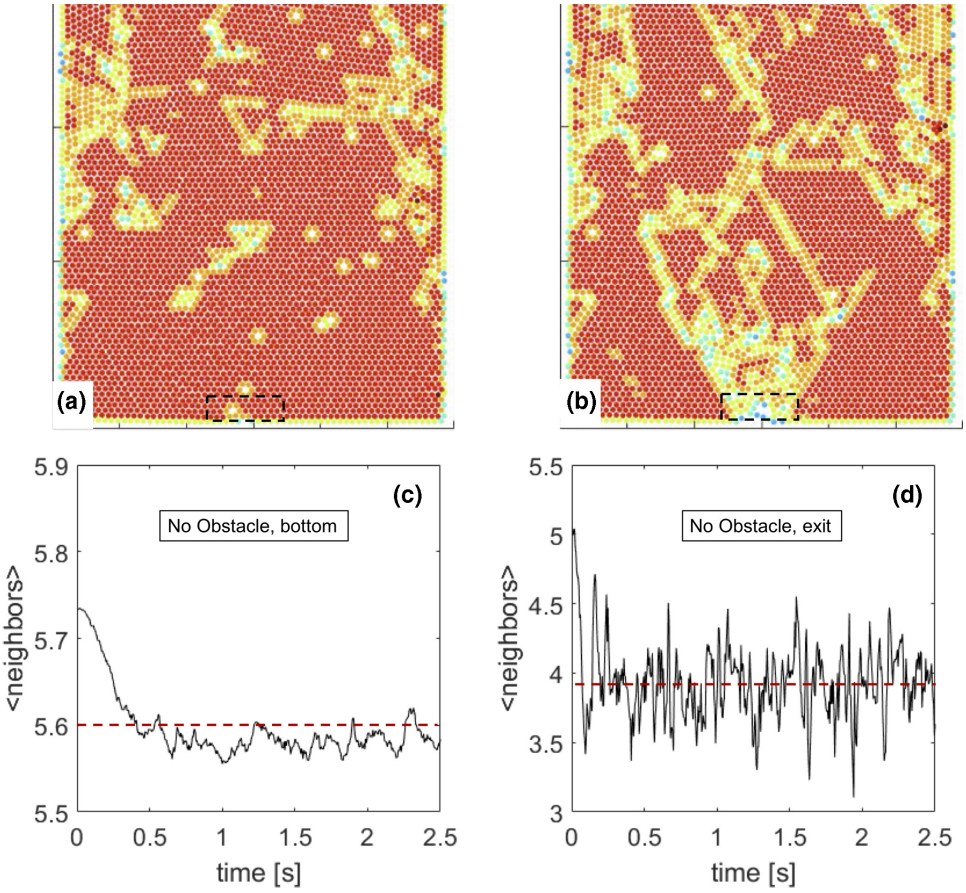

FIG. 6. The packing for $t = 0$ s (a) and $t = 1$ s (b) with no obstacle present. Red particles have six neighbors; other colors in general have less than six neighbors. The dashed box indicates the "exit" region. The average neighbor number vs time for the bottom of the silo (c) and the exit (d). After a transient upon startup, both values have a steady mean with some fluctuations. The mean for the bottom is 5.60 ± 0.039 and the mean for the exit is 3.93 ± 0.275.

has a mass flow profile [6] with stagnant corner regions as expected for this geometry. In Fig. 4(b), we see an instantaneous picture of particle speeds, which show a fairly symmetric distribution and are not dissimilar from Fig. 4(a). In Fig. 4(c), we see that after a transient, the particles move with a characteristic speed, though there are significant temporal fluctuations. We also see these temporal fluctuations in time sequences of plots like Fig. 4(b).

The horizontal granular temperature is in Fig. 5, for both the bottom of the silo, as well as the exit region. We see that the mean granular temperature is $(1.31 \pm 0.481) \times 10^4$ mm^2/s^2 at the bottom of the silo. The mean value is $(1.46 \pm 0.606) \times 10^5$ mm^2/s^2 near the exit, an order of magnitude higher than the overall average.

The neighbor count is depicted in Fig. 6. The top images show neighbor counts for the intiial packing ($t = 0$) and for $t = 1$ s. We see that the bottom of the silo has a fairly regular packing initially with some defects. Upon flow, more defects are present, but they are localized to the exit region. The typical number of neighbors is five or six, given an average of 5.60 ± 0.039. In the exit region, the neighbor count is substantially lower, with an average of 3.93 ± 0.275. *Case 2: Obstacle size* $= 10D$. The velocity field is shown in Fig. 7. In Fig. 7(a), tracks are overlain to show

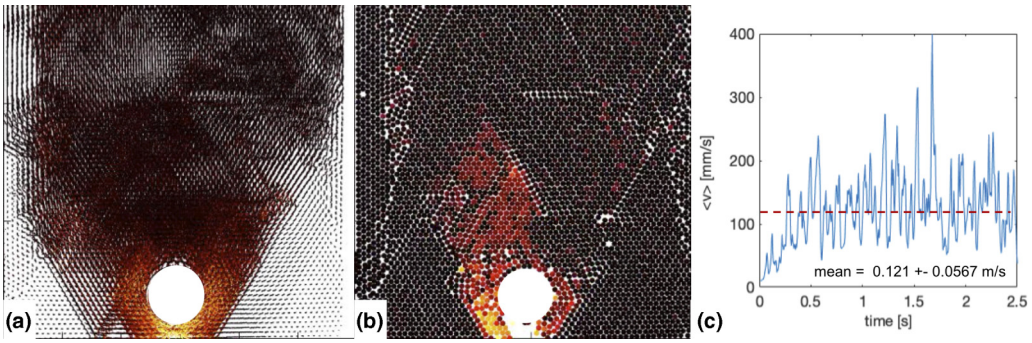

FIG. 7. (a) Tracks for 2.5 s of flow in the 10D experiment, overlain to show the particle movement and active/inactive regions. (b) Instantaneous speed at $t = 1$ s, with the same color scale. (C) Average particle speed vs time for the 10D obstacle experiment.

the particle motion. Again, most motion is near the aperture. We note that the stagnant zones once again appear as in the no obstacle case. There is a slight (8%) decrease in average speed compared to the no obstacle case. The transient behavior and fluctuations are not remarkably different.

The horizontal granular temperature is in Fig. 8, for both the bottom of the silo, as well as the exit region. We see that the mean granular temperature is $(1.66 \pm 0.606) \times 10^4$ mm^2/s^2 at the bottom of the silo. The mean value is $(7.41 \pm 2.35) \times 10^5$ mm^2/s^2 near the exit. As with the case of no obstacle, the exit temperature is larger than the bulk temperature. However, notably the exit temperature is substantially larger than the bulk case (about a fivefold increase).

The neighbor count is depicted in Fig. 9. The top images show neighbor counts for the initial packing ($t = 0$) and for $t = 1$ s and $t = 2$ s. We see that the bottom of the silo has some initial defects introduced by the intruder. However, these defects are local to the obstacle. The typical number of neighbors in the bulk is still five or six, given an average of 5.67 ± 0.0360, which is indistinguishable from the no obstacle case. The exit neighbor count is about 13% lower than the no obstacle case, with an average of 3.43 ± 0.316; however, this is not surprising given that the obstacle geometrically frustrates particles from packing tighter.

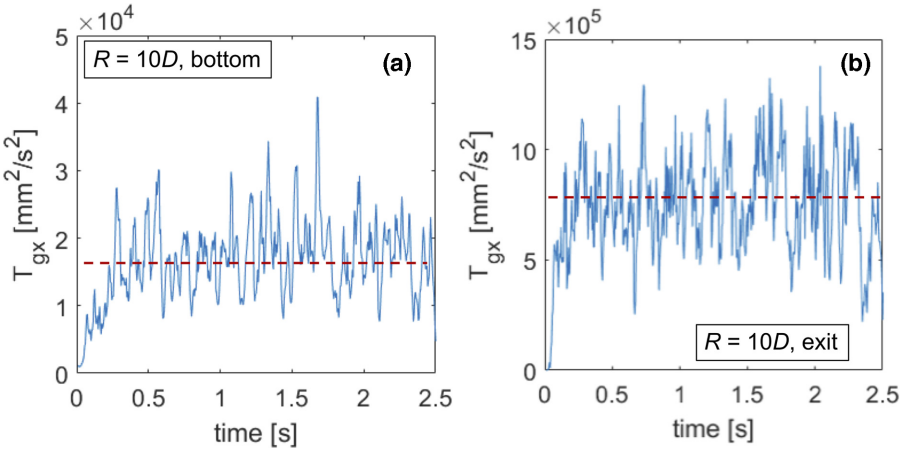

FIG. 8. (a) The horizontal granular temperature at the bottom of the silo for the 10D obstacle case. The mean value is $(1.66 \pm 0.606) \times 10^4$ mm^2/s^2. (b) The horizontal granular temperature at the exit of the silo. The mean value is $(7.41 \pm 2.35) \times 10^5$ mm^2/s^2.

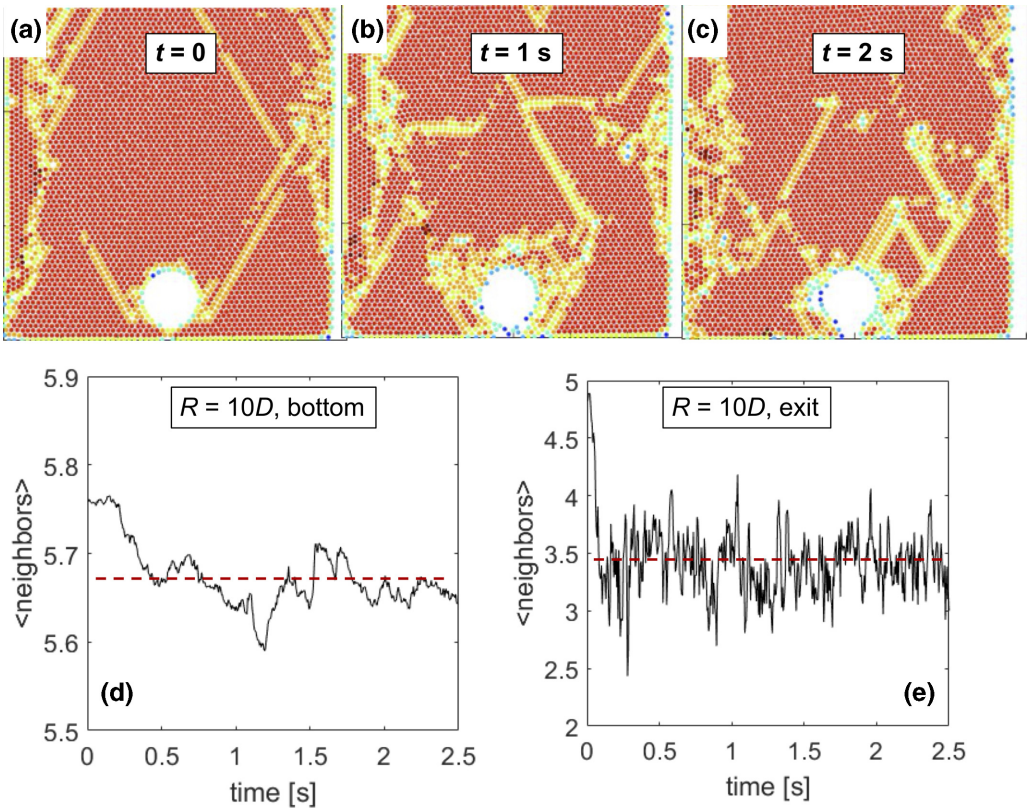

FIG. 9. (a),(b),(c) The packing for $t = 0$ s, $t = 1$ s, and $t = 2$ s with a $10D$ obstacle. While the obstacle creates some disorder, it is more localized than in the $30D$ case. Red particles have six neighbors; all other colors have less than six neighbors. There are some rare seven-neighbored particles (dark red) as the tolerance for neighbor selection was 10% higher than the particle size. The average neighbor number vs time for the bottom of the silo (d) and the exit (e). The mean for the bottom is 5.67 ± 0.0360; the mean for the exit is 3.43 ± 0.316.

Case 3: Obstacle size $= 17D$. The velocity field is shown in Fig. 10. In Fig. 10(a), tracks are overlain to show the particle motion. Again, most motion is near the aperture, with stagnant zones as before. However, looking at Figs. 10(a) and 10(b), one can see more detouring type motion around the obstacle, resulting in more horizontal trajectories at the aperture. This detouring also appears to slow everything down further, with a reduction in overall speed of about 12% from the no obstacle case.

The horizontal granular temperature is in Fig. 11, for both the bottom of the silo, as well as the exit region. We see that the mean granular temperature is $(2.11 \pm 1.21) \times 10^4$ mm^2/s^2 at the bottom of the silo. The mean value is $(4.73 \pm 1.41) \times 10^5$ mm^2/s^2 near the exit. These two findings are interesting in comparison to the $10D$ case. The bulk temperature is larger, suggesting the larger obstacle induces more overall horizontal velocity fluctuations. This is not surprising as there is a larger fixed object to collide with. However, these fluctuations at the exit are over 50% smaller, indicating less dynamic fluidity, which makes sense considering the propensity of this case to clog.

The neighbor count is depicted in Fig. 12. The top images show neighbor counts for the initial packing ($t = 0$) and for $t = 1$ s and $t = 2$ s. We see that the bottom of the silo has some initial defects introduced by the obstacle, but much like in $10D$ appear local. The typical number of neighbors in bulk has not changed significantly (5.61 ± 0.022) nor has the exit value changed from the $10D$ case (3.40 ± 0.320).

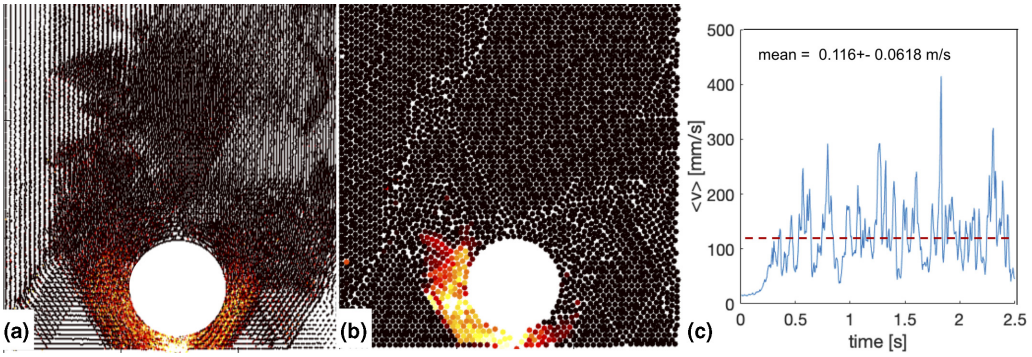

FIG. 10. (a) Tracks for 2.5 s of flow in the 17D experiment, overlain to show the particle movement and active/inactive regions. (b) Instantaneous speed at $t = 1$ s, with the same color scale. (c) Average particle speed vs time for the 17D obstacle experiment.

Case 4: Obstacle size $= 30D$. The velocity field is shown in Fig. 13. In Fig. 13(a), tracks are overlain to show the particle motion. Most motion occurs near the aperture again but there are several interesting features to highlight. The first is that the stagnant zones in the bottom corner are almost gone. The second is the presence of a stagnation zone at the top of the obstacle. This is likely a mechanical effect; particles near this region are pressed into the obstacle, making a somewhat rigid structure. This acts as an additional structure to detour moving particles to either side. This seems to be a similar phenomenon to "dynamic" dunes, as seen in [26], though further study is needed. Lastly we note an overall larger particle velocity, about 34% larger than the no obstacle case.

The horizontal granular temperature is in Fig. 14, for both the bottom of the silo, as well as the exit region. We see that the mean granular temperature is $(3.24 \pm 1.45) \times 10^4$ mm^2/s^2 at the bottom of the silo. The mean value is $(1.13 \pm 0.422) \times 10^6$ mm^2/s^2 near the exit. The bulk temperature keeps growing as the obstacle size increases, and the exit temperature is larger than the 10D case.

The neighbor count is depicted in Fig. 15. The top images show neighbor counts for the initial packing ($t = 0$) and for $t = 1$ s and $t = 2$ s. We see that the bottom of the silo has some initial defects

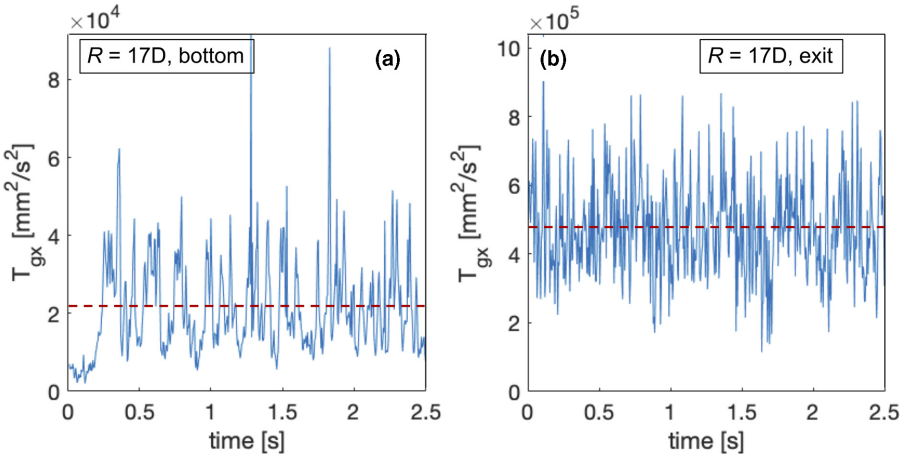

FIG. 11. (a) The horizontal granular temperature at the bottom of the silo for the 17D obstacle case. The mean value is $(2.11 \pm 1.21) \times 10^4$ mm^2/s^2. (b) The horizontal granular temperature at the exit of the silo. The mean value is $(4.73 \pm 1.41) \times 10^5$ mm^2/s^2.

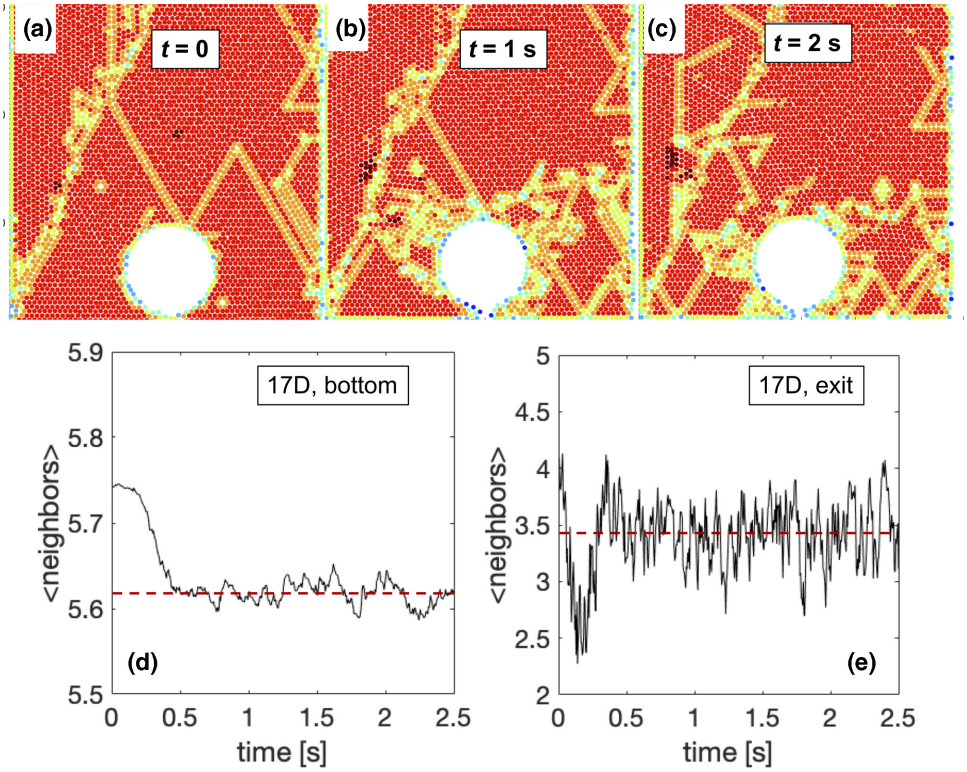

FIG. 12. (a),(b),(c) The packing for $t = 0$ s, $t = 1$ s, and $t = 2$ s with a $17D$ obstacle. While the obstacle creates some disorder, it is more localized than in the $30D$ case. Red particles have six neighbors; all other colors have less than six neighbors. There are some rare seven-neighbored particles (dark red) as the tolerance for neighbor selection was 10% higher than the particle size. Bottom: the average neighbor number vs time for the bottom of the silo (d) and the exit (e). The mean for the bottom is 5.61 ± 0.022 and the mean for the exit is (3.40 ± 0.320).

introduced by the intruder. As the flow develops, the defects spread and eventually span the system. The typical number of neighbors in the bulk is still five or six, with an average of 5.43 ± 0.0681; however, this is statistically different from the other cases, and the standard deviation is about two times larger. The exit region is statistically identical to the other obstacle cases, with an average of 3.49 ± 0.381.

V. DISCUSSION

In prior work, there have been several mechanisms proposed to understand clog suppression, some of which may operate together, making them difficult to separate. One simple mechanism is that of geometrical suppression: an intruder will prevent a clogging arch at the top of the aperture. However, by specifically focusing on cases of obstacles near the aperture, we have accepted that this is an effect: we do not expect a spanning arch above the outlet as it would be statistically unlikely for a keystone particle at the center to get to the proper position. By accepting this mechanism as already in effect, we can further delineate mechanisms of clog suppression, as these systems may still form clogs on the sides. Another mechanism that has been proposed is a reduction in the pressure at the outlet, specifically that the obstacle reduces the vertical velocity and results in less competition to the exit. Another possibly related mechanism is detouring of particles: they move around the obstacle and collide below the obstacle, thus raising the granular temperature of the

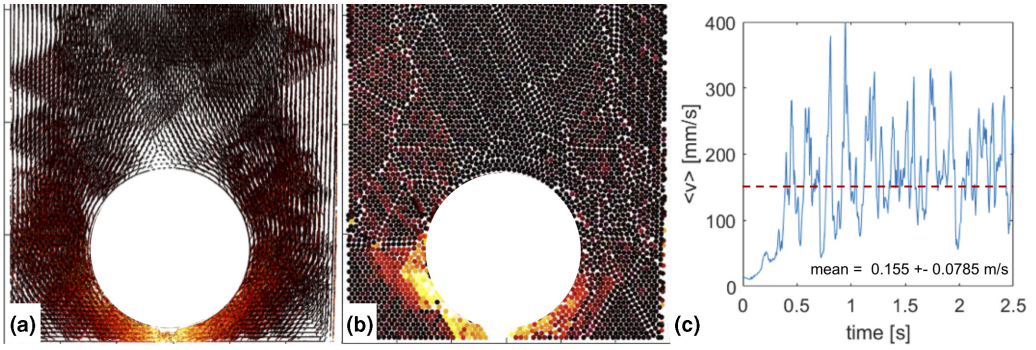

FIG. 13. (a) Tracks for 2.5 s of flow in the 30D experiment, overlain to show the particle movement and active/inactive regions. (b) Instantaneous speed at $t = 1$ s, with the same color scale. (c) Average particle speed vs time for the 30D obstacle experiment.

region below the obstacle and reducing the packing fraction. For circular obstacles, the packing fraction was found to be reduced below the obstacle when the obstacle is close to the aperture. However, obstacles further away result in packing fractions below the obstacle that are relatively the same as in the bulk.

In our experiments, we have observed trends in the data with respect to obstacle size, summarized in Figs. 16 and 17. We present each graph reminding the reader of the bulk trend: no obstacle cases clog with high probability, 10D never clogs, 17D clogs with high probability, and 30D rarely clogs. We start by discussing obvious conclusions, then move on to individual cases.

We first can see, comparing Fig. 16(a) to 16(b), that the horizontal granular temperature is greater near the exit aperture than in the bulk in all cases. This is not surprising in itself, as particles are colliding in that region, giving randomness to their motion. Also, the bulk horizontal granular temperature increases monotonically with increasing obstacle size, shown in Fig. 16(a). As mentioned earlier in this paper, this is a trend that makes perfect sense: there is a larger fixed object with which to collide—so more fluctuations from bouncing should occur. It is reassuring that there is a systematic effect with obstacle size. However, the temperature near the exit for 17D is smaller

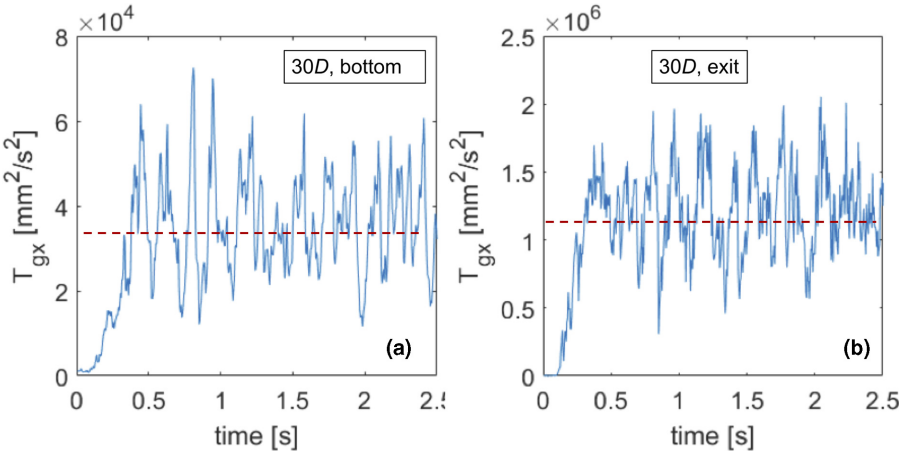

FIG. 14. (a) The horizontal granular temperature at the bottom of the silo for the 30D obstacle case. The mean value is $(3.24 \pm 1.45) \times 10^4$ mm^2/s^2. (b) The horizontal granular temperature at the exit of the silo. The mean value is $(1.13 \pm 0.422) \times 10^6$ mm^2/s^2.

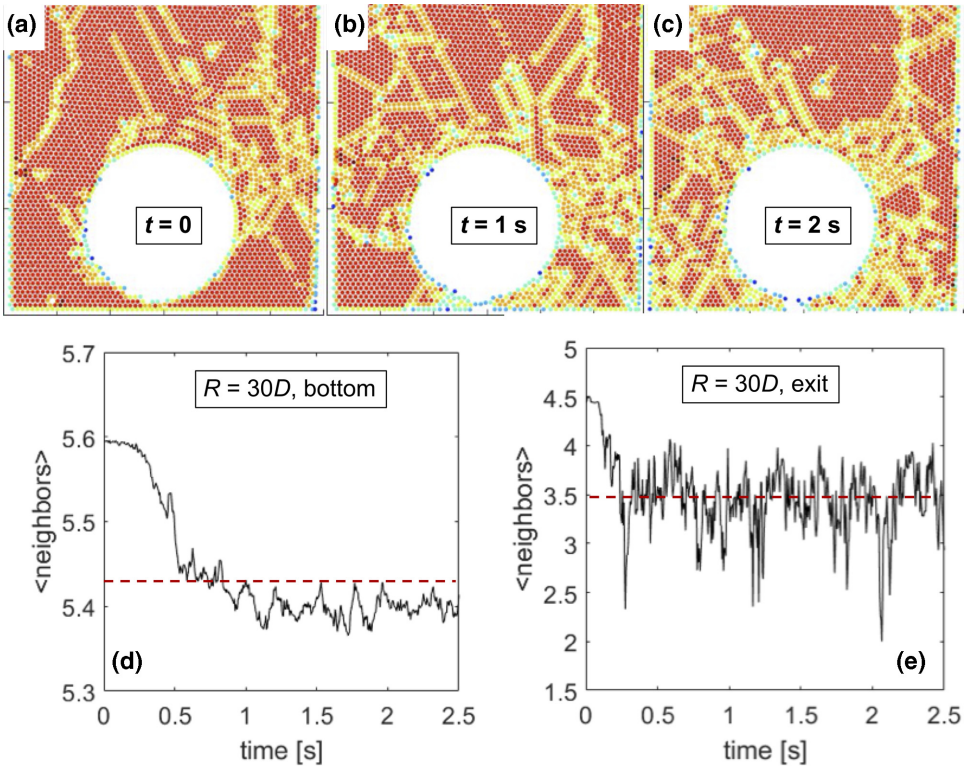

FIG. 15. (a),(b),(c) The packing for $t = 0$ s, $t = 1$ s, and $t = 2$ s with a $30D$ obstacle, showing the spread of disorder in the system. Red particles have six neighbors; other colors have less than six neighbors. There are some rare seven-neighbored particles (dark red) as the tolerance for neighbor selection was 10% higher than the particle size. Bottom: The average neighbor number vs time for the bottom of the silo (d) and the exit (e). The mean for the bottom is 5.43 ± 0.0681; the mean for the exit is 3.49 ± 0.381.

than both $10D$ and $30D$, which points to a reason for the high clogging likelihood: the material is much less "fluid" for that case and so is less likely to "spontaneously" unjam. $10D$ does not have a substantial side bottleneck area, and the obstacle stymies "normal" clogging, so it makes sense that this case is more fluid and does not clog. However, both $17D$ and $30D$ have side bottleneck regions, so the mystery is why the $30D$ case is more fluid.

Indeed, when looking at other measurements, the $30D$ case is exceptional. The average instantaneous particle speed in $30D$ is measurably larger than the other cases [Fig. 17(a)], indicating a more freely flowing system. Adding an obstacle in general seems to reduce the average neighbor number [Fig. 17(b), pink] near the exit, but this is a geometric effect and there seems to be no difference between the obstacle cases. The bulk count [Fig. 17(b), green] is at first glance unaffected by the obstacle. This is similar to looking at the packing fraction in previous work, where little difference was found. However, the $30D$ does have a slightly lower bulk neighbor count, albeit only slightly—one might be hard pressed to even claim it is significant. While small changes in packing fraction can have large effects on overall dynamics, in practice it may be difficult to register this as a significant change. So again we see a difference in the details for the three obstacle cases, which is most easily seen by disaggregating the data from the averages.

Specifically, by looking at the map of neighbor counts, we see that disorder is localized in the no obstacle, $10D$, and $17D$ cases, while it spreads throughout the system for the $30D$ case. A caveat to this is that the defect structure cannot be disentangled from the monodispersity of the packing or the

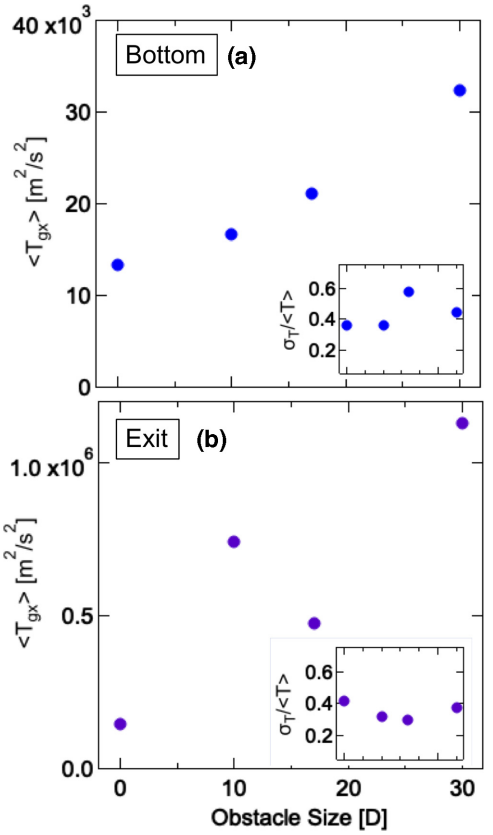

FIG. 16. (a) Horizontal granular temperature in the bottom of the silo vs obstacle size. (No obstacle = 0D.) (b) Temperature in the exit region vs obstacle size.

boundary conditions. In fact, disentangling these effects is an important problem for future study. However, since these remain the same for these experiments, we can at least compare between these trials and we see that based on the defect structure, the entire system is also structurally more fluid for 30D. Effectively, there seems to be just enough extra space for particles to move and bounce off each other, resulting in a higher granular temperature and less clogging.

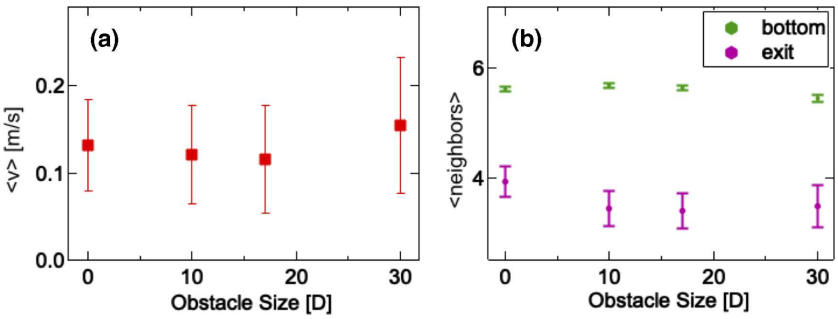

FIG. 17. (a) Average instantaneous speed of particles in the bottom of the silo vs obstacle size. (No obstacle = 0D.) (b) Average neighbor count vs obstacle size. Green markers refer to the entire bottom region; pink to the exit region.

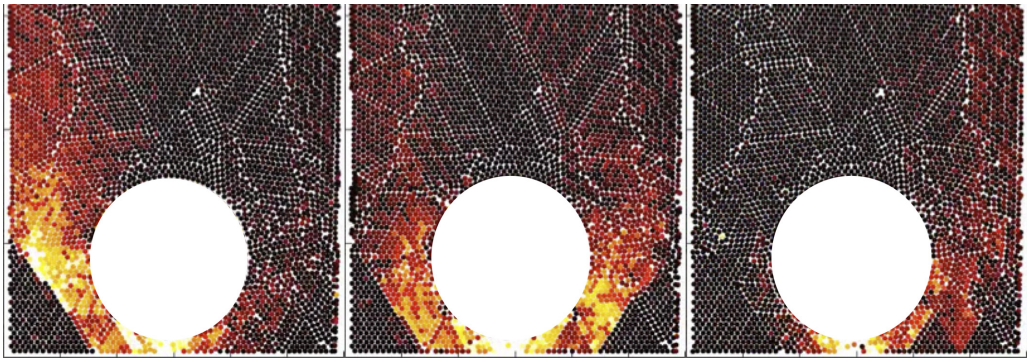

FIG. 18. A visualization of asymmetric flows we see in the obstacle experiments. Left: Flow primarily on the left side; the right side is halted around this time. This image also shows plastic deformation along grain boundaries further from the obstacle and exit. Center: A "burst" mode, where both sides flow with speeds higher than average. Right: Flow dominated by the right side.

To recap, we did not see clogging for the $10D$ case, but this is quite consistent with other results [19]. The narrow region that might count as a side bottleneck is infinitesimally small for $10D$, and it is statistically unlikely for a standard clog to occur. However, for $17D$ we see clogging very often, because the lower curvature of the obstacle creates a longer bottleneck. $30D$ has an even longer bottleneck, but we do not see clogging very often. However, $30D$ will disturb the packing order more than $17D$, creating a larger granular temperature. So the particles in $17D$ do not end up with enough exit temperature to suppress clogging events; one can explicitly see this temperature reduction in Fig. 16(b).

Thus what we see is not exclusively structure or dynamics, it is both: a structural property (the obstacle) makes a structural disturbance in the granular material which affects the particle dynamics. Further, this disturbance can propagate quite far into the material. We have proposed a better metric (the neighbor count) to measure the packing than the packing fraction, as disordered and underpacked regions are quite spatially heterogeneous: there is no one packing fraction in these systems, especially near the obstacle and exit where boundaries may be ill-defined. A proposed next set of experiments is to study how this disorder percolation length scale might grow with obstacle size, and how obstacle shape might affect these results, as a triangle, for instance, could complement the packing order rather than frustrating it [21].

Another open set of questions regards the prevalence of asymmetric, intermittent flows, as illustrated in Fig. 18. These flows were also seen in [21], but we were not able to come up with a reliable metric to characterize them. They appear to occur unpredictably. We do see some intermittent asymmetry in the no obstacle case, but the presence is exaggerated with the obstacles. Further investigations with photoelastic particles should shed light on why this phenomenon occurs. While it does not appear that these flow details affect the bulk flow rate [21] substantially, this would have an impact on an individual particle's "experience." Indeed, one could design different systems where clogging is likely or unlikely, by choosing some combination of aperture size, obstacle size, or position, and even tune different systems so that the bulk rate is roughly the same. But a similar flow rate may come at the cost of some particles getting stuck or slowing down. If the goal is a homogeneous flow, this must be considered, and certainly should be considered if designing pedestrian or traffic systems.

Lastly, it is to be determined how general these results are. Ignoring the temptation to compare particles to pedestrians, we ask an even more basic question. Do these results follow in 3D, do they follow with "real" granular (polydisperse, angular, etc.) materials? What about the effects of gravity, which would be different when mining asteroids or sampling sands on Mars. Presumably the value of g plays a major role, and yet it can be challenging to vary in a satisfying way experimentally. This

points to an open door for important simulation work, in the absence of an open door onto a space shuttle.

ACKNOWLEDGMENTS

The authors thank L. McEachern and T. Liimatainen for technical support. This work is partially funded by ACS PRF Award No. 56888-UN19, by the Research Corporation for Science Advancement Award No. 24516, and by NSF CAREER Award No. 1846991.

[1] C. Mankoc, A. Janda, R. Arevalo, J. M. Pastor, I. Zuriguel, A. Garcimartin, and D. Maza, The flow rate of granular materials through an orifice, Granular Matter **9**, 407 (2007).
[2] L. Kondic, Simulations of two dimensional hopper flow, Granular Matter **16**, 235 (2014).
[3] X. Hong, M. Kohne, M. Morrell, H. Wang, and E. R. Weeks, Clogging of soft particles in two-dimensional hoppers, Phys. Rev. E **96**, 062605 (2017).
[4] A. Janda, I. Zuriguel, and D. Maza, Flow Rate of Particles through Apertures Obtained from Self-Similar Density and Velocity Profiles, Phys. Rev. Lett. **108**, 248001 (2012).
[5] R. Stannarius, D. Sancho Martinez, T. Finger, E. Somfai, and T. Börzsönyi, Packing and flow profiles of soft grains in 3D silos reconstructed with x-ray computed tomography, Granular Matter **21**, 56 (2019).
[6] L. Fullard, D. J. Holland, P. Galvosas, C. Davies, P.-Y. Lagrée, and S. Popinet, Quantifying silo flow using MRI velocimetry for testing granular flow models, Phys. Rev. Fluids **4**, 074302 (2019).
[7] I. Zuriguel, D. R. Parisi, R. C. Hidalgo, C. Lozano, A. Janda, P. A. Gago, J. P. Peralta, L. M. Ferrer, L. A. Pugnaloni, E. Clément, D. Maza, I. Pagonabarraga, and A. Garcimartín, Clogging transition of many-particle systems flowing through bottlenecks, Sci. Rep. **4**, 7324 (2014).
[8] H. Péter, A. Libál, C. Reichhardt, and C. J. O. Reichhardt, Crossover from jamming to clogging behaviours in heterogeneous environments, Sci. Rep. **8**, 10252 (2018).
[9] J. M. Pastor, A. Garcimartín, P. A. Gago, J. P. Peralta, C. Martín-Gómez, L. M. Ferrer, D. Maza, D. R. Parisi, L. A. Pugnaloni, and I. Zuriguel, Experimental proof of faster-is-slower in systems of frictional particles flowing through constrictions, Phys. Rev. E **92**, 062817 (2015).
[10] D. Helbing, L. Buzna, A. Johansson, and T. Werner, Self-organized pedestrian crowd dynamics: Experiments, simulations, and design solutions, Transp. Sci. **39**, 1 (2005).
[11] D. Helbing, A. Johansson, J. Mathiesen, M. H. Jensen, and A. Hansen, Analytical Approach to Continuous and Intermittent Bottleneck Flows, Phys. Rev. Lett. **97**, 168001 (2006).
[12] R. Nedderman, U. Tuzun, S. Savage, and G. Houlsby, Simulations of two dimensional hopper flow, J. Chem. Eng. Sci. **37**, 1597 (1982).
[13] K. To, P.-Y. Lai, and H. K. Pak, Jamming of Granular Flow in a Two-Dimensional Hopper, Phys. Rev. Lett. **86**, 71 (2001).
[14] K. To, Jamming transition in two-dimensional hoppers and silos, Phys. Rev. E **71**, 060301(R) (2005).
[15] A. Janda, I. Zuriguel, A. Garcimartín, L. A. Pugnaloni, and D. Maza, Jamming and critical outlet size in the discharge of a two-dimensional silo, Europhys. Lett. **84**, 44002 (2008).
[16] C. C. Thomas and D. J. Durian, Geometry dependence of the clogging transition in tilted hoppers, Phys. Rev. E **87**, 052201 (2013).
[17] I. Zuriguel, Invited review: Clogging of granular materials in bottlenecks, Pap. Phys. **6**, 060014 (2014).
[18] C. C. Thomas and D. J. Durian, Fraction of Clogging Configurations Sampled by Granular Hopper Flow, Phys. Rev. Lett. **114**, 178001 (2015).
[19] I. Zuriguel, A. Janda, A. Garcimartín, C. Lozano, R. Arévalo, and D. Maza, Silo Clogging Reduction by the Presence of an Obstacle, Phys. Rev. Lett. **107**, 278001 (2011).
[20] C. Lozano, A. Janda, A. Garcimartín, D. Maza, and I. Zuriguel, Flow and clogging in a silo with an obstacle above the orifice, Phys. Rev. E **86**, 031306 (2012).
[21] K. Endo, K. A. Reddy, and H. Katsuragi, Obstacle-shape effect in a two-dimensional granular silo flow field, Phys. Rev. Fluids **2**, 094302 (2017).

[22] G. Cai, A. B. Harada, and K. N. Nordstrom, Mesoscale metrics on approach to the clogging point, Granular Matter **23**, 69 (2021).
[23] J. C. Crocker and D. G. Grier, Methods of digital video microscopy for colloidal studies, J. Colloid Interface Sci. **179**, 298 (1996).
[24] E. Thackray and K. Nordstrom, Gravity-driven granular flow in a silo: Characterizing local forces and rearrangements, EPJ Web Conf. **140**, 03087 (2017).
[25] T. Matsushima and R. Blumenfeld, Universal Structural Characteristics of Planar Granular Packs, Phys. Rev. Lett. **112**, 098003 (2014).
[26] Y. Amarouchene, J. F. Boudet, and H. Kellay, Dynamic Sand Dunes, Phys. Rev. Lett. **86**, 4286 (2001).